Phase diagram of the half-filled two-dimensional SU(N) Hubbard-Heisenberg model: a quantum Monte Carlo study.

F.F. Assaad
Institut für Theoretische Physik und Astrophysik Universität Würzburg, Am Hubland D-97074 Würzburg

We investigate the phase diagram of the half-filled $SU(N)$ Hubbard-Heisenberg model with hopping t, exchange J and Hubbard U, on a two-dimensional square lattice. In the large-N limit, and as a function of decreasing values of t/J, the model shows a transition from a d-density wave state to a spin dimerized insulator. A similar behavior is observed at $N = 6$ whereas at $N = 2$ a spin density wave insulating ground state is stabilized. The $N = 4$ model, has a d-density wave ground state at large values of t/J which as a function of decreasing values of t/J becomes unstable to an insulating state with no apparent lattice and spin broken symmetries. In this state, the staggered spin-spin correlations decay as a power-law, resulting in gapless spin excitations at $\vec{q} = (\pi, \pi)$. Furthermore, low lying spin modes with small spectral weight are apparent around the wave vectors $\vec{q} = (0, \pi)$ and $\vec{q} = (\pi, 0)$. This gapless spin liquid state is equally found in the $SU(4)$ Heisenberg ($U/t \to \infty$) model in the self-adjoint antisymmetric representation. An interpretation of this state in terms of a π-flux phase is offered. Our results stem from projective ($T = 0$) quantum Monte-Carlo simulations on lattice sizes ranging up to 24×24.

PACS numbers: 71.27.+a, 71.10.-w, 71.10.Fd

I. INTRODUCTION

$SU(N)$ symmetric models of correlated electron systems have attracted considerable interests in the past decades. For instance, those models are relevant for the understanding of Mott insulators with orbital degeneracy as described by the Kugel-Khomskii Hamiltonian [1]. For two-fold orbital degeneracy and at a point where the orbital and spin degrees of freedom play a very symmetric role, this model maps onto an $SU(4)$ symmetric Hubbard, or Heisenberg model with fundamental representation on each site [2]. It has also recently been argued that realizations of $SU(N)$ Hubbard models are at reach in the context of optical lattices [3].

$SU(N)$ generalizations of $SU(2)$ lattice fermion models can be solved exactly in the large-N limit. Systematic corrections in terms of Gaussian fluctuations around the mean-field or saddle point solution may be computed. The simplifications which occur in the large-N limit, namely the suppression of quantum fluctuations have important consequences for auxiliary field quantum Monte Carlo (QMC) simulations. As a function of growing values of N the negative sign problem inherent to stochastic methods is reduced thus rendering simulations more and more tractable. In fact, some generalizations of Hubbard models lead to the absence of sign problems for specific values of N and irrespective of doping [4, 5]. However, the extrapolation from the soluble large-N limit to the physical $N = 2$ case is by no means unambiguous since phase transitions can occur as a function of N.

In this article, we will primarily concentrate on the half-filled Hubbard-Heisenberg model on a square lattice and map out it's phase diagram as a function of N and coupling strength. At this band filling, the sign problem is absent for even values of N. Hence, ground state properties can be investigated on lattice sizes ranging up to 24×24 unit cells. We will show the existence of d-density wave (DDW) states down to $N = 4$ and of spin-dimerized states at $N = 6$. The most intriguing result is a possible realization of a gapless spin-liquid phase for the $N = 4$ model in the Heisenberg limit.

The $SU(N)$ symmetric Hubbard-Heisenberg model we consider reads:

$$\begin{aligned} H &= H_t + H_U + H_J \quad \text{with} \\ H_t &= -t \sum_{\langle \vec{i},\vec{j} \rangle} \vec{c}^{\dagger}_{\vec{i}} \vec{c}_{\vec{j}} + \text{H.c.} \\ H_U &= \frac{U}{N} \sum_{\vec{i}} \left(\vec{c}^{\dagger}_{\vec{i}} \vec{c}_{\vec{i}} - \rho \frac{N}{2} \right)^2 \\ H_J &= -\frac{J}{2N} \sum_{\langle \vec{i},\vec{j} \rangle} \left(D^{\dagger}_{\vec{i},\vec{j}} D_{\vec{i},\vec{j}} + D_{\vec{i},\vec{j}} D^{\dagger}_{\vec{i},\vec{j}} \right). \end{aligned} \tag{1}$$

Here, $\vec{c}^{\dagger}_{\vec{i}} = (c^{\dagger}_{\vec{i},1}, c^{\dagger}_{\vec{i},2}, \cdots, c^{\dagger}_{\vec{i},N})$ is an N-flavored spinor, $D_{\vec{i},\vec{j}} = \vec{c}^{\dagger}_{\vec{i}} \vec{c}_{\vec{j}}$ and ρ corresponds to the band-filling. At $N = 2$, the operator identity

$$\begin{aligned} \frac{-1}{4} \quad & \left(D^{\dagger}_{\vec{i},\vec{j}} D_{\vec{i},\vec{j}} + D_{\vec{i},\vec{j}} D^{\dagger}_{\vec{i},\vec{j}} \right) = \\ & \vec{S}_{\vec{i}} \cdot \vec{S}_{\vec{j}} + \frac{1}{4} \left[(n_{\vec{i}} - 1)(n_{\vec{j}} - 1) - 1 \right] \end{aligned} \tag{2}$$

holds. Here, the fermionic representation of the spin 1/2 operator reads $\vec{S} = \frac{1}{2} \sum_{s,s'} c^{\dagger}_{s} \vec{\sigma}_{s,s'} c_{s'}$ where $\vec{\sigma}$ are the Pauli spin matrices. Thus, at $N = 2$ the model reduces to the standard Hubbard-Heisenberg model.

In the strong coupling limit, $U/t \to \infty$, and at integer values of $\rho N/2$, charge fluctuations are suppressed. The model maps onto the $SU(N)$ Heisenberg Hamiltonian

$$H = \frac{J}{N} \sum_{\langle \vec{i},\vec{j} \rangle} \sum_{\alpha,\beta} S_{\alpha,\beta,\vec{i}} S_{\beta,\alpha,\vec{j}} \tag{3}$$

with

$$S_{\alpha,\beta,\vec{i}} = c^{\dagger}_{\alpha,\vec{i}} c_{\beta,\vec{i}} - \frac{1}{N}\delta_{\alpha,\beta}\sum_{\gamma} c^{\dagger}_{\gamma,\vec{i}} c_{\gamma,\vec{i}} \tag{4}$$

the generators of $SU(N)$ satisfying the commutation relations:

$$\left[S_{\alpha,\beta,\vec{i}}, S_{\gamma,\delta,\vec{j}}\right] = \delta_{\vec{i},\vec{j}}\left(S_{\alpha,\delta,\vec{i}}\delta_{\gamma,\beta} - S_{\gamma,\beta,\vec{i}}\delta_{\alpha,\delta}\right). \tag{5}$$

The representation of the $SU(N)$ group is determined by the local constraint

$$\vec{c}^{\dagger}_{\vec{i}}\vec{c}_{\vec{i}} = \rho\frac{N}{2}. \tag{6}$$

In the terminology of Young tableaux the above leads to a tableau with $\rho N/2$ rows and a single column. In particular, at $N = 4$, and $\rho = 1/2$ (quarter band-filling) the model maps onto the $SU(4)$ symmetric Kugel-Khomskii Hamiltonian with fundamental representation of $SU(4)$ on each lattice site. A study of large-N Heisenberg models in various representations may be found in Ref. [6].

$SU(N)$ Heisenberg models have been considered numerically in Refs. [7, 8]. Those models differ substantially from ours in the choice of the representation. On one sublattice the fundamental representation (Young tableau with one row and a single column) is considered and on the other the adjoint representation (Young tableau with $N-1$ rows and a single column). Based on Green function Monte-Carlo methods, it has been argued this $SU(4)$ model has a spin-liquid ground state. However, simulations on larger lattice sizes with the loop algorithm have shown that the model has a broken symmetry ground state [8]. In contrast, our results for the $SU(4)$ Heisenberg model, at $\rho = 1$ and in the self-adjoint representation (see Eq. (6)) point towards an insulating state with no broken symmetries.

The article is organized as follows. In the next section we formulate the the partition function of the model as a path integral over bosonic field. This formulation constitutes the starting point for both the saddle point approximation and the auxiliary field quantum Monte Carlo simulations. In Section III we present the phase diagram of the half-filled model as a function of N and coupling constants. Finally, we summarize and draw conclusions.

II. LARGE-N LIMIT AND QUANTUM MONTE-CARLO SIMULATION.

Both the saddle point approximation as well as the auxiliary field QMC rely on a path integral formulation of the partition function. Using the Trotter decomposition, we write the partition function as:

$$Z = \mathrm{Tr}\left[e^{-\beta H}\right] = \mathrm{Tr}\left[\prod_{n=1}^{m} e^{-\Delta\tau H_t} e^{-\Delta\tau H_U} e^{-\Delta\tau H_J}\right] \tag{7}$$

Here $m\Delta\tau = \beta$ and we have omitted the systematic error of oder $\Delta\tau^2$. Using the Hubbard Stratonovich (HS) transformation, we introduce bosonic fields to decouple the two body interaction terms. Let us start with the Heisenberg term which we write – replacing the sum over nearest neighbors $\langle\vec{i},\vec{j}\rangle$ by a sum over bonds b - in terms of perfect squares

$$H_J = -\frac{J}{4N}\sum_b \left(D^{\dagger}_b + D_b\right)^2 - \left(D^{\dagger}_b - D_b\right)^2. \tag{8}$$

We can now apply the standard HS transformation to obtain:

$$\begin{aligned} e^{-\Delta\tau H_J} &\propto \int\prod_b \mathrm{d}\gamma_b \mathrm{d}\eta_b \qquad (9)\\ &e^{-\sum_b\left[\frac{\gamma_b^2}{2}+\frac{\eta_b^2}{2}-\sqrt{\frac{J\Delta\tau}{2N}}\left(\gamma_b(D^{\dagger}_b+D_b)+i\eta_b(D^{\dagger}_b-D_b)\right)\right]}\\ &\propto \int\prod_b \mathrm{dRe}z_b\mathrm{dIm}z_b e^{-\sum_b\left[N\Delta\tau J|z_b|^2-\Delta\tau J\left(z_b D^{\dagger}_b+\bar{z}_b D_b\right)\right]}. \end{aligned}$$

In the above, we introduce a complex variable per bond: $z_b = (\gamma_b + i\eta_b)/\sqrt{2NJ\Delta\tau}$. Following the same steps, we decouple the Hubbard term as:

$$e^{-\Delta\tau H_U} \propto \int\prod_{\vec{i}} \mathrm{d}\Phi_{\vec{i}} e^{-\sum_{\vec{i}}\left[N\Delta\tau U\Phi^2_{\vec{i}}/4 - i\Delta\tau U\Phi_{\vec{i}}\left(\vec{c}^{\dagger}_{\vec{i}}\vec{c}_{\vec{i}}-\rho N/2\right)\right]}. \tag{10}$$

Using the above transformations, the partition function in the limit $\Delta\tau \to 0$ is given by a functional integral over the space and imaginary time dependent HS fields:

$$Z \propto \int\prod_{\vec{i}}\mathrm{D}\Phi_{\vec{i}}(\tau)\prod_b \mathrm{DRe}z_b(\tau)\mathrm{DIm}z_b(\tau) e^{-NS(\{\Phi\},\{z\},\{\bar{z}\})}. \tag{11}$$

The action reads:

$$\begin{aligned} S\left(\{\Phi\},\{z\},\{\bar{z}\}\right) &= \underbrace{\int \mathrm{d}\tau J\sum_b |z_b(\tau)|^2 + U\sum_{\vec{i}}\Phi^2_{\vec{i}}(\tau)/4}_{=S_0}\\ &\quad - \ln\mathrm{Tr}\left[T e^{-\int_0^\beta \mathrm{d}\tau h(\tau)}\right]. \qquad (12) \end{aligned}$$

with

$$\begin{aligned} h(\tau) &= -\sum_{\langle\vec{i},\vec{j}\rangle}\left[\left(t + J\bar{z}_{\langle\vec{i},\vec{j}\rangle}(\tau)\right)c^{\dagger}_{\vec{i}}c_{\vec{j}} + \mathrm{H.c.}\right]\\ &\quad -iU\sum_{\vec{i}}\Phi_{\vec{i}}(\tau)\left(c^{\dagger}_{\vec{i}}c_{\vec{i}} - \rho/2\right) \qquad (13) \end{aligned}$$

Notice that in the above definition of $h(\tau)$, the creation and annihilation operators are not N-flavored spinors but correspond to spinless fermion operators.

A. The Saddle point.

In the large-N limit, the saddle point approximation,

$$\frac{\delta S}{\delta z_b(\tau)} = \frac{\delta S}{\delta \bar{z}_b(\tau)} = \frac{\delta S}{\delta\Phi_{\vec{i}}(\tau)} = 0 \tag{14}$$

becomes exact. Assuming time independent fields, we derive the mean-field equations:

$$\begin{aligned} \Phi_{\vec{i}} &= i\left(2\langle c^\dagger_{\vec{i}} c_{\vec{i}}\rangle_h - \rho\right) \\ z_{\langle\vec{i},\vec{j}\rangle} &= \langle c^\dagger_{\vec{i}} c_{\vec{j}}\rangle_h \\ \bar{z}_{\langle\vec{i},\vec{j}\rangle} &= \langle c^\dagger_{\vec{j}} c_{\vec{i}}\rangle_h . \end{aligned} \tag{15}$$

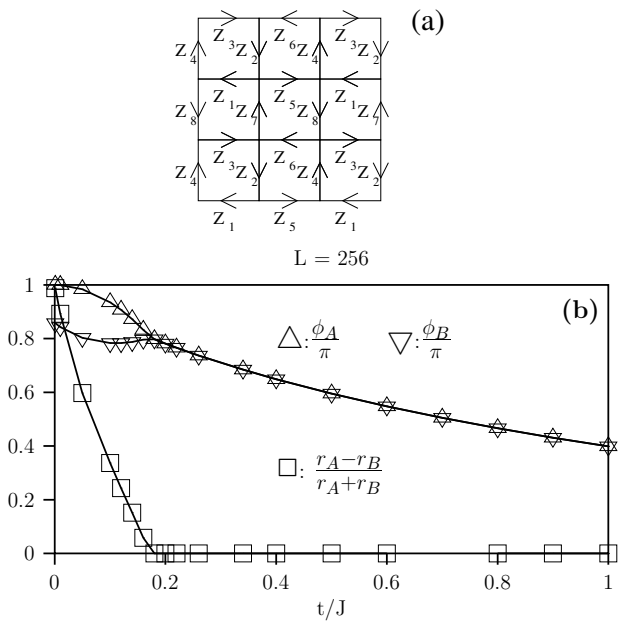

FIG. 1: (a) The four site unit cell with lattice vectors, $\vec{a}_1 = 2\vec{a}_x$ and $\vec{a}_2 = 2\vec{a}_y$ and corresponding fields. Here, $\vec{a}_x$ and $\vec{a}_y$ correspond to the lattice vectors of the underlying square lattice. (b) Mean-field order parameters (see Eq. 17) as obtained from the saddle point equations.

The above saddle point has been considered by Affleck and Marston [9, 10]. At half-band filling, $\rho = 1$, and *large* values of t/J a d-density wave state is realized. This state becomes unstable towards dimerization as the coupling t/J is reduced. Here, we have solved the mean-field equations for a four site unit-cell (see Fig. 1), thus allowing more freedom in the dimerization pattern than in [10]. With

$$Z_i \equiv r_i e^{i\phi_i/4}, \tag{16}$$

the solutions we find are characterized by:

$$\begin{aligned} r_1 = r_2 = r_3 = r_4 = r_A, r_5 = r_6 = r_7 = r_8 = r_B \\ \phi_1 = \phi_2 = \phi_3 = \phi_4 = \phi_A, \phi_5 = \phi_6 = \phi_7 = \phi_8 = \phi_B . \end{aligned} \tag{17}$$

The values of the oder parameters are plotted in Fig. 1. As apparent the d-density wave state with $r_A = r_B$ and $\phi_A = \phi_B$ is unstable towards box dimerization below $t_c/J \simeq 0.17$ [11]. The DDW state is a semi-metal since gapless single particle excitations are present at wave vectors $(\pm\pi/2a, \pm\pi/2a)$. Dimerization opens a quasiparticle gap at all wave vectors. Hence the transition from the DDW to the dimerized phase corresponds to a semi-metal to insulator transition as shown in Fig. 2.

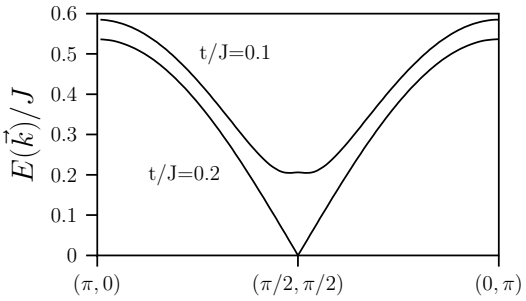

FIG. 2: Lowest lying single particle excitation at half-band filling. The transition from the DDW state to dimerized state corresponds to a semi-metal to insulator transition.

We note that the results of Affleck and Marston [10] may be recovered by imposing:

$$Z_5 = Z_3, Z_6 = Z_1, Z_7 = Z_4, \text{ and } Z_8 = Z_2. \tag{18}$$

B. The Monte Carlo simulation.

The Monte-Carlo approach relies on the same formulation of the partition function. Before discussing details of the implementation let us concentrate on our primary concern, namely the sign problem. In general, $e^{-NS(\phi,z,\bar{z})}$ is not a positive quantity and hence may not be interpreted as an unnormalized probability distribution from which we sample field configurations. Hence, in the Monte Carlo method, we consider the probability distribution:

$$P(\phi, z, \bar{z}) = \frac{\left|e^{-NS(\phi,z,\bar{z})}\right|}{\int \mathcal{D}\left[\phi, z, \bar{z}\right] \left|e^{-NS(\phi,z,\bar{z})}\right|} \tag{19}$$

and estimate the expectation value of an observable with:

$$\langle O\rangle = \frac{\int \mathcal{D}\left[\phi, z, \bar{z}\right] P(\phi, z, \bar{z}) e^{i\delta(\phi,z,\bar{z})} O(\phi, z, \bar{z})}{\int \mathcal{D}\left[\phi, z, \bar{z}\right] P(\phi, z, \bar{z}) e^{i\delta(\phi,z,\bar{z})}}. \tag{20}$$

In the above, $O(\phi, z, \bar{z})$ is the expectation value of the observable for a given configuration of fields, and $e^{-NS(\phi,z,\bar{z})} = \left|e^{-NS(\phi,z,\bar{z})}\right| e^{i\delta(\phi,z,\bar{z})}$. The denominator in the above equation, corresponds to the average sign: $\langle e^{i\delta}\rangle_P$.

In the large-N limit, where the saddle point approximation becomes exact, the average sign is temperature independent and equal to unity. On the other hand, it is known that for the SU(2) model the average sign decays as $e^{-\Delta V\beta}$ where V corresponds to the volume of the system and Δ is a positive constant. Hence, we can conjecture that Δ is a decreasing function of N. This has for consequence that at a given temperature the sign problem becomes less and less severe as function of growing

values of N. We have checked this numerically for the quarter filled, $\rho = 1/2$, model. Unfortunately the sign problem for the $SU(4)$ quarter-filled model – the $SU(4)$ symmetric Kugel-Khomskii model – was still to severe to study the nature of the Mott insulating phase in the strong coupling limit.

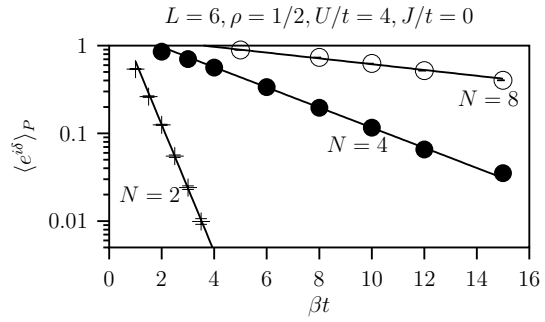

FIG. 3: Average sign as a function of N for the quarter-filled $SU(N)$ Hubbard model. The solid line corresponds to a fit to the form: $ae^{-b\beta}$.

At half-band filling, $\rho = 1$, and even values of N, particle-hole symmetry leads to the absence of a minus-sign problem. At this filling, and under the canonical transformation

$$c_{\vec{i}}^{\dagger} \rightarrow (-1)^{i_x + i_y} c_{\vec{i}} \tag{21}$$

the Hamiltonian $h(\tau)$ transforms as:

$$h(\tau) \rightarrow \overline{h(\tau)} \tag{22}$$

such that

$$\mathrm{Tr}\left[T e^{-\int_0^\beta \mathrm{d}\tau h(\tau)} \right] = \overline{\mathrm{Tr}\left[T e^{-\int_0^\beta \mathrm{d}\tau h(\tau)} \right]}. \tag{23}$$

Hence, the above quantity is real and

$$e^{-NS} = e^{-NS_0} \left[\mathrm{Tr}\left[T e^{-\int_0^\beta \mathrm{d}\tau h(\tau)} \right] \right]^N \tag{24}$$

is positive for even values of N.

We now summarize the technicalities required to carry efficient simulations. Since we are interested in ground state properties, it is more efficient to adopt a projective method based on the equation:

$$\langle O \rangle_0 = \lim_{\beta \rightarrow \infty} \frac{\langle \Psi_T | e^{-\beta H/2} O e^{-\beta H/2} | \Psi_T \rangle}{\langle \Psi_T | e^{-\beta H} | \Psi_T \rangle}. \tag{25}$$

The trial wave function $|\Psi_T\rangle$ is required to be non-orthogonal to the ground state and β corresponds to a projection parameter. For the trial wave function we choose the form:

$$|\Psi_T\rangle = |\Psi_T\rangle_1 \otimes |\Psi_T\rangle_2 \otimes \cdots \otimes |\Psi_T\rangle_N \tag{26}$$

where $|\Psi_T\rangle_\alpha$ is the ground state of the single particle Hamiltonian $-t \sum_{\langle \vec{i},\vec{j} \rangle} c_{\vec{i},\alpha}^{\dagger} c_{\vec{j},\alpha} + \mathrm{H.c.}$ in the flavor α Hilbert space. With this choice of trial wave function, the action within the projection formalism takes the form:

$$S = S_0 - \ln \langle \chi_T | T e^{-\int_0^\beta \mathrm{d}\tau h(\tau)} | \chi_T \rangle \tag{27}$$

where $|\chi_T\rangle$ is the ground state of the spinless fermion Hamiltonian: $-t \sum_{\langle \vec{i},\vec{j} \rangle} c_{\vec{i}}^{\dagger} c_{\vec{j}} + \mathrm{H.c.}$. In the simulations we will present in the next section, we have typically used $\beta J = 40$ which we found to be sufficient to filter out the ground state from the trial wave function within statistical uncertainty.

We use a finite imaginary time-step $\Delta\tau$ which we have set to $\Delta\tau J = 0.1$. This introduces a systematic error of the order $\Delta\tau^2$. Given this systematic error, it is much more efficient to use an approximate discrete HS transformation to decouple the perfect square term:

$$e^{\Delta\tau\lambda A^2} = \sum_{l=\pm1,\pm2} \gamma(l) e^{\sqrt{\Delta\tau\lambda}\eta(l)A} + \mathcal{O}(\Delta\tau^4) \tag{28}$$

where the fields η and γ take the values:

$$\gamma(\pm1) = 1 + \sqrt{6}/3, \;\; \gamma(\pm2) = 1 - \sqrt{6}/3$$
$$\eta(\pm1) = \pm\sqrt{2\left(3 - \sqrt{6}\right)}, \;\; \eta(\pm2) = \pm\sqrt{2\left(3 + \sqrt{6}\right)}.$$

This transformation is not exact and produces an overall systematic error proportional to $(\Delta\tau\lambda)^3$ in the Monte Carlo estimate of an observable. However, since we already have a systematic error proportional to $\Delta\tau^2$ from the Trotter decomposition, the transformation is as good as exact. It has the great advantage of being discrete thus allowing efficient sampling.

C. The Heisenberg limit.

We conclude this technical part with some comments concerning the numerical simulations of the Heisenberg model. At $t/J = 0$, H_U is a good quantum number since $[H_{tUJ}, H_U] = 0$. Hence, in principle it suffices to choose a trial wave function $|\Psi_T\rangle$ satisfying $H_U|\Psi_T\rangle = 0$ to guarantee that the imaginary time propagation converges to the ground state of the Heisenberg model (see Eq. 25). On the other hand, one can relax this constraint on the trial wave function and implement a Gutzwiller projection onto the Hilbert space with no double occupancy. We have found the second approach to be much more efficient.

The algorithm we use here is very related to the one we have used in Ref. [12] where a detailed technical section is provided.

III. NUMERICAL RESULTS

Our results are summarized in the phase diagram shown in Fig. 4. Here, we consider the half-filled case

as a function of N and t/J. For values of $t/J > 0$ we set $U = 0$. The $t = 0$ line corresponds to the Heisenberg model where charge fluctuations are completely suppressed (see Sec. II C). In the large-N limit, the data stems for the mean-field calculation of the previous section. At $N = 6$, we essentially reproduce the saddle point result with a somewhat smaller value of t_c/J reflecting the instability of the DDW phase in favor of the spin-dimerized phase. Irrespective of the coupling t/J, the $SU(2)$ model shows an insulating spin-density wave (SDW) state. The most interesting feature of the phase diagram occurs at $N = 4$. Apart from the DDW phase present at *large* values of t/J we find an insulating phase (solid circles in Fig. 4) with no apparent broken symmetries and no spin gap. We will argue that in this phase the antiferromagnetic spin correlations are critical leading to gapless spin modes around the antiferromagnetic wave vector $\vec{Q} = (\pi, \pi)$. Furthermore, we will present results showing that low lying spin modes with very small spectral weight are present around the $\vec{q} = (0, \pi)$ and $\vec{q} = (0, \pi)$ wave vectors. Before proceeding let us remind the reader that our simulations are carried out with the projective algorithm of Eq. 25 and hence reflect ground state properties.

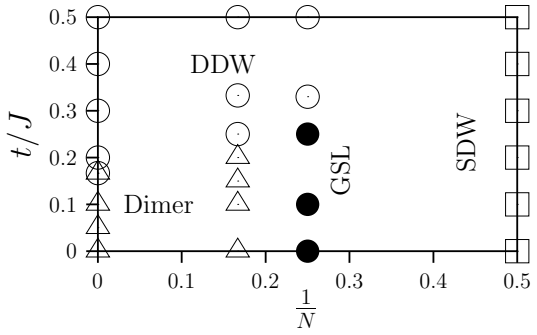

FIG. 4: Phase diagram of the half-filled (i.e. $\rho = \frac{2}{N}\sum_\alpha \langle c^\dagger_{\vec{i},\alpha} c_{\vec{i},\alpha}\rangle$) Hubbard-Heisenberg model as a function of t/J. For $t/J > 0$ we set $U = 0$. The $t = 0$ line corresponds to the Heisenberg model where charge fluctuations are completely suppressed (see Sec. II C). The symbols correspond to the parameters where we have carried out simulations and denote the following phases: △: Spin-dimerized phase, ◯: DDW phase, □: Spin-density wave phase, and •: insulating phase with no broken lattice and spin symmetries and no gap to spin excitations (gapless spin-liquid (GSL) phase).

To establish the above phase diagram, we have computed equal-time and time displaced correlation functions. Let $O(\vec{i})$ be an observable, with time displaced correlation function:

$$S_O(\vec{i} - \vec{j}, \tau) = \langle O(\vec{i}, \tau) O(\vec{j})\rangle - \langle O(\vec{i})\rangle\langle O(\vec{j})\rangle \tag{29}$$

and corresponding Fourier transform:

$$S_O(\vec{q}, \tau) = \sum_{\vec{r}} e^{i\vec{q}\vec{r}} S_O(\vec{r}, \tau). \tag{30}$$

From the equal time correlation function $S_O(\vec{q}) \equiv S_O(\vec{q}, \tau = 0)$, we can establish the presence of long range order at a given wave vector. In this case $S_O(\vec{q})$ scales as the volume of the system, V, the proportionality constant being the square of the order-parameter. From the imaginary time displaced correlation functions, we can compute spectral functions, $S_O(\vec{q}, \omega)$, by solving,

$$\begin{aligned} S_O(\vec{q}, \tau) &= \frac{1}{\pi}\int \mathrm{d}\omega S_O(\vec{q}, \omega) e^{-\tau\omega}, \\ S_O(\vec{q}) &= \frac{1}{\pi}\int \mathrm{d}\omega S_O(\vec{q}, \omega), \end{aligned} \tag{31}$$

with the use of the Maximum Entropy method.

Information on gaps and the spectral weight of the lowest lying excitation, is obtained directly form the imaginary time correlation function without having recourse to analytical continuation.

$$\begin{aligned} S_O(\vec{q}, \tau) &= \sum_n |\langle\Psi_0|O(-\vec{q})|\chi_n(\vec{q})\rangle|^2 e^{-\tau(E_n(\vec{q}) - E_0)} \\ &\stackrel{\tau\to\infty}{\longrightarrow} \underbrace{|\langle\Psi_0|O(-\vec{q})|\chi_0(\vec{q})\rangle|^2}_{Z_O(\vec{q})} e^{-\Delta_O(\vec{q})\tau}. \end{aligned} \tag{32}$$

In the above, $|\Psi_0\rangle$ corresponds to the normalized ground state. $|\chi_n(\vec{q})\rangle$ are eigenstates of H with momentum $\vec{q}$ and $|\langle\Psi_0|O(-\vec{q})|\chi_n(\vec{q})\rangle| > 0$. The gap $\Delta_O(\vec{q})$ corresponds to the energy difference between the first excited state $|\chi_0(\vec{q})\rangle$ and the ground state and $O(\vec{q}) = \frac{1}{\sqrt{V}}\sum_{\vec{j}} e^{i\vec{q}\vec{j}} O(\vec{j})$. Finally, the residue $Z_O(\vec{q})$ corresponds to the spectral weight of the lowest lying excitation.

To study the model, we have considered the following observables. Let us define the magnetization as

$$O_{\mathrm{spin}}(\vec{i}) = \sum_\alpha f(\alpha) c^\dagger_\alpha c_\alpha \;\text{ with }\; \sum_\alpha f(\alpha) = 0. \tag{33}$$

For even values of N considered here, we choose $f(\alpha) = \pm 1$. Note that $SU(N)$ symmetry leads to the identity

$$S_{\mathrm{spin}}(\vec{i}-\vec{j}) \equiv \langle O_{\mathrm{spin}}(\vec{i}) O_{\mathrm{spin}}(\vec{j})\rangle = \frac{N}{N^2-1}\langle\sum_{\alpha,\beta} S_{\alpha,\beta,\vec{i}} S_{\beta,\alpha,\vec{j}}\rangle \tag{34}$$

where $S^{\alpha,\beta}_{\vec{i}}$ are the generators of $SU(N)$ (See Eq. 4).

To detect spin-dimerization and DDW instabilities we consider respectively

$$O_{\mathrm{dimer}}(\vec{i}) = O_{\mathrm{spin}}(\vec{i}) O_{\mathrm{spin}}(\vec{i} + \vec{a}_x) \tag{35}$$

and

$$O_{\mathrm{DDW}}(\vec{i}) = j_x(\vec{i}) - j_y(\vec{i}) \tag{36}$$

with current:

$$j_x(\vec{i}) = i\sum_\alpha \left(c^\dagger_{\vec{i},\alpha} c_{\vec{i}+\vec{a}_x,\alpha} - c^\dagger_{\vec{i}+\vec{a}_x,\alpha} c_{\vec{i},\alpha}\right) \tag{37}$$

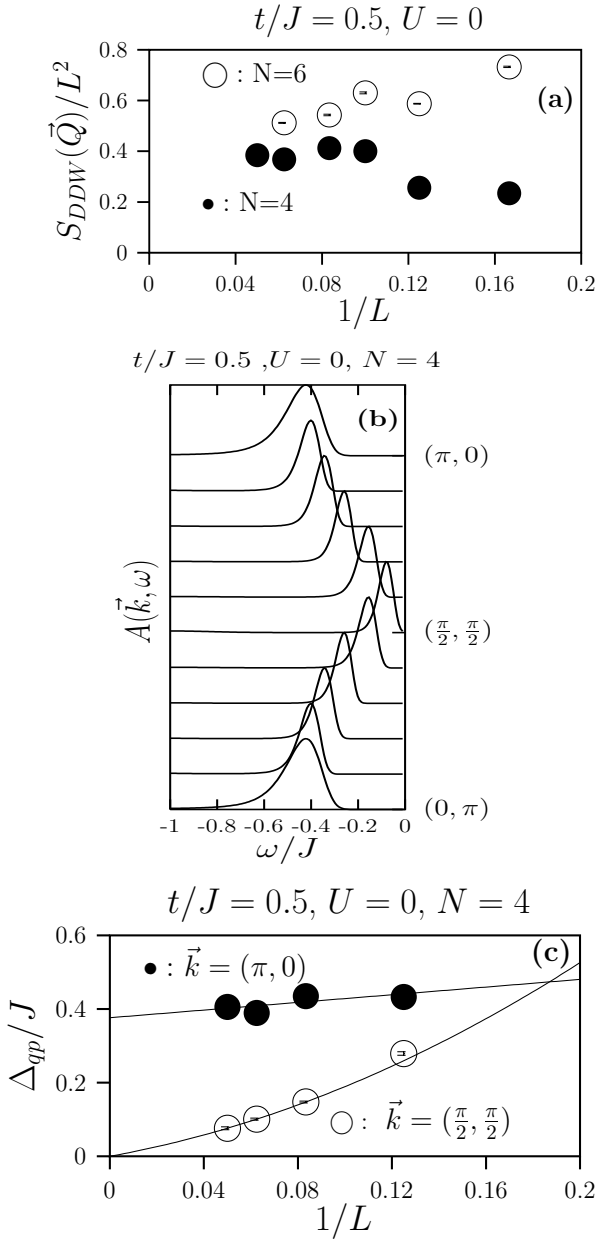

FIG. 5: (a) Size scaling of the DDW equal time correlation functions at wave vector $\vec{Q} = (\pi, \pi)$. (b) Single particle spectral function in the DDW phase on a 20×20 lattice. Here, we normailze the peak height to unity and along the $(0, \pi)$ to $(\pi, 0)$ line each spectrum satisfies the sum-rule $\int_{-\infty}^{0} \mathrm{d}\omega A(\vec{k}, \omega) = \pi n(\vec{k}) = \pi/2$. (c) Size scaling of the quasiparticle gap at $\vec{k} = (\pi/2, \pi/2)$ and $\vec{k} = (0, \pi)$. The data shows the semi-metal character of the DDW phase.

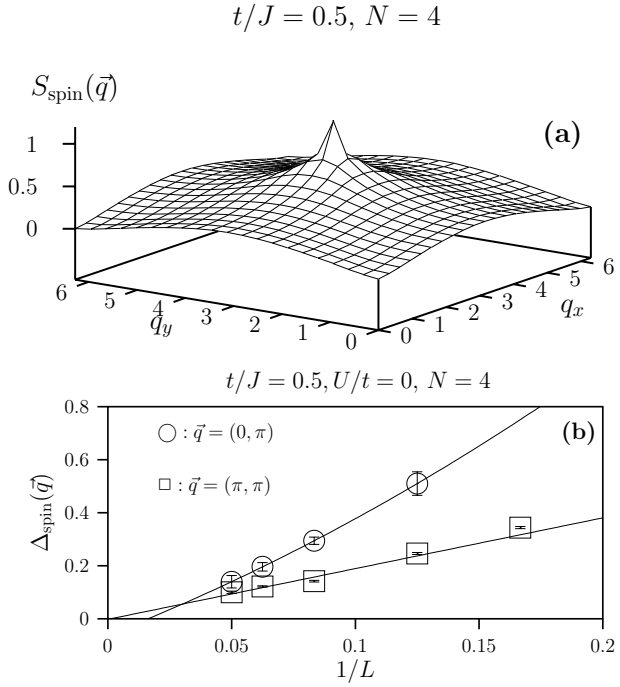

FIG. 6: Spin correlations in the DDW phase. a) Equal time spin structure factor. b) Size scaling of the spin gap at $\vec{q} = (0, \pi)$ and $\vec{q} = (\pi, \pi)$.

and an equivalent form for $j_y(\vec{i})$. Finally, we obtain information on single particle excitations by measuring time displaced Green functions: $G(\vec{k}, \tau) = -\langle T c_{\vec{k},\alpha}(\tau) c^{\dagger}_{\vec{k},\alpha}(0) \rangle$. From this quantity we can extract quasiparticle gaps as well as the spectral function $A(\vec{k}, \omega)$.

A. The DDW phase

We start our description of the phase diagram with the DDW phase. Fig. 5a shows the finite size scaling of $S_{\rm DDW}(\vec{Q})/L^2$ at the antiferromagnetic wave vector $\vec{Q} = (\pi, \pi)$. For $t/J = 0.5$ and both considered values of N the data supports $\lim_{L\to\infty} S_{\rm DDW}(\vec{Q})/L^2 > 0$ thus signaling a DDW ordered phase. One can confirm this point of view from the analysis on the single particle spectral function along the $\vec{k} = (0, \pi)$ to $\vec{k} = (\pi, 0)$ line in the Brillouin zone (see Fig. 5b). After size scaling (see Fig. 5c) the data is consistent with the vanishing of the quasiparticle gap at $\vec{k} = (\pi/2, \pi/2)$ thus confirming the semi-metal character of the DDW phase.

Since the single particle spectrum has gapless excitations at the nodal points $\vec{k} = (\pm\pi/2, \pm\pi/2)$ we can expect gapless spin excitations centered around the wave vectors $\vec{q} = (0, \pi)$, $\vec{q} = (\pi, 0)$ and $\vec{q} = (\pi, \pi)$, along with a power-law decay of the equal time spin-spin correlations. Fig. 6 confirms this. The spin gap vanishes at the above mentioned wave vectors (Fig. 6b). The spectral weight, $Z_{\rm spin}(\vec{q})$, of the low lying $\vec{q} = (0, \pi)$ spin excitation is very small in comparison to $\vec{q} = (\pi, \pi)$. For the $L = 20$ lattice we have $Z_{\rm spin}(\vec{q})/S_{\rm spin}(\vec{q}) \simeq 0.006$ at $\vec{q} = (0, \pi)$ and $Z_{\rm spin}(\vec{q})/S_{\rm spin}(\vec{q}) \simeq 0.5$ at $\vec{q} = (\pi, \pi)$. The data on which this statement is based stems from Fig. 12c. The size

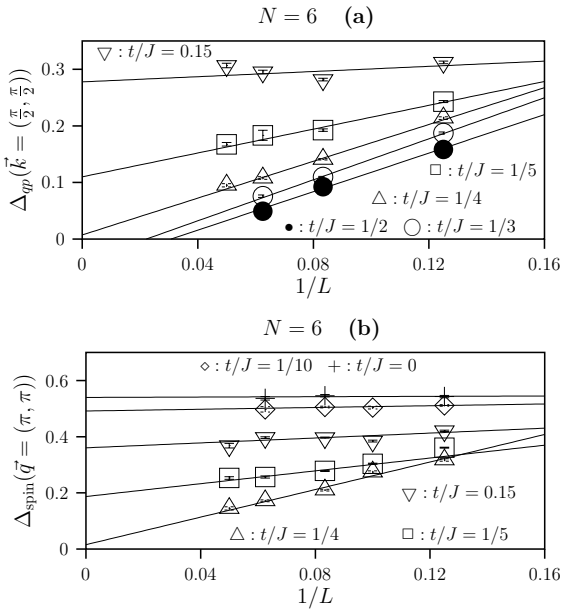

FIG. 7: Quasiparticle (a) and spin (b) gaps at $N = 6$ as a function of coupling. For $t/J > 0$ we set $U = 0$, and $t/J = 0$ refers to the Heisenberg model (see Sec. II C).

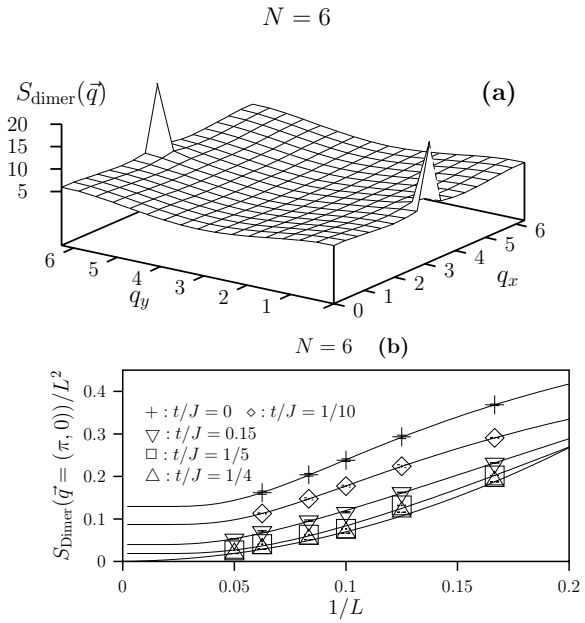

FIG. 8: (a) Equal time dimer correlation functions for the $SU(6)$ Heisenberg model. (b) Size scaling of the dimer correlation function at $\vec{q} = (0, \pi)$. For $t/J > 0$ we set $U = 0$, and $t/J = 0$ refers to the Heisenberg model (see Sec. II C).

scaling of the static spin structure factor at $\vec{Q} = (\pi, \pi)$ is consistent with a power-law decay of the staggered spin-spin correlation functions: $S_{\rm spin}(\vec{Q} = (\pi, \pi))/L^2 \propto L^{-2}$. It is interesting to note that even though gapless spin excitations are present at $\vec{q} = (0, \pi)$ no sign of a cusp in the spin structure factor at this wave vector is apparent (See Fig. 6a). This signals a *large* exponent for the $(0, \pi)$ spin correlations. Note that in the saddle approximation both the $(0, \pi)$ and (π, π) spin correlations decay as r^{-4} and no cusp feature in the static spin structure factor is apparent [13].

B. N=6

To study the stability of the DDW phase from $t/J = 0.5$ to the Heisenberg point, it is convenient to consider the quasiparticle gap at $\vec{k} = (\pi/2, \pi/2)$ (see Fig. 7a). For values of $t/J \leq 1/5$ the data is consistent with the opening of a quasiparticle gap at $\vec{k} = (\pi/2, \pi/2)$. The opening of the quasiparticle gap is accompanied by the opening of a spin-gap (see 7b). Hence, the data suggest that for values of $t/J \leq 1/5$ at $N = 6$ we have entered a spin dimerized phase, with spin and charge gaps.

We confirm this point of view by looking into the dimer correlation functions (see Fig. 8a). Those correlations are dominant at wave vector $\vec{q} = (\pi, 0)$ in agreement with the mean-field dimerization pattern. To establish long-range order we have to extrapolate $S_{\rm dimer}(\pi, 0)/L^2$ to the thermodynamic limit. For $t/J \leq 1/5$ gaps are present both in the charge and spin degrees of freedom. Since the presence of gaps is equivalent to the localization of spin and charge degrees of freedom, we fit the finite size data to the form: $a + br^c e^{-L/\xi}$. Adopting this form for the finite size corrections, the data is consistent with the onset of a spin-dimerized state for $t/J \leq 1/5$.

C. N=4

We now turn our attention to the $SU(4)$ model. From the size analysis of the quasiparticle gap at $\vec{k} = (\pi/2, \pi/2)$ (see Fig. 9a) we can conclude that the DDW state is unstable for values of $t/J \leq 1/4$. In contrast to the $N = 6$ case, no spin gap opens across the transition up to the Heisenberg limit (see Fig. 9b). The correlation functions presented in Fig. 10 in the Heisenberg limit show dominant spin-spin correlations. In accordance with the absence of spin gap no sign of long-range dimerization is apparent.

The issue is now to establish the existence or non-existence of long range antiferromagnetic order. In Fig. 11, we plot the spin-spin correlation at the largest distance, $(L/2, L/2)$, on our $L \times L$ lattice as well as $S_{\rm spin}(\vec{q} = (\pi, \pi))/L^2$ as a function of $1/L$. As apparent, the extrapolation is consistent with the absence of long-range magnetic ordering. In particular, at the Heisenberg point, where we have carried out simulations on lattices ranging up to 24×24, our extrapolated values read $\lim_{L\to\infty} S_{\rm spin}(\vec{r} = (L/2, L/2)) = 0.002 \pm 0.003$ along with $\lim_{L\to\infty} S_{\rm spin}(\vec{Q} = (\pi, \pi))/L^2 = 0.0008 \pm 0.004$.

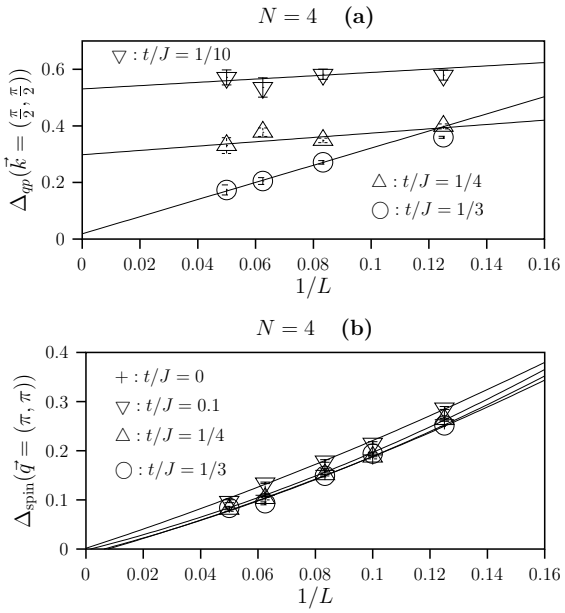

FIG. 9: Size scaling of the quasiparticle and spin gaps at $N = 4$. For $t/J > 0$ we set $U = 0$, and $t/J = 0$ refers to the Heisenberg model (see Sec. II C).

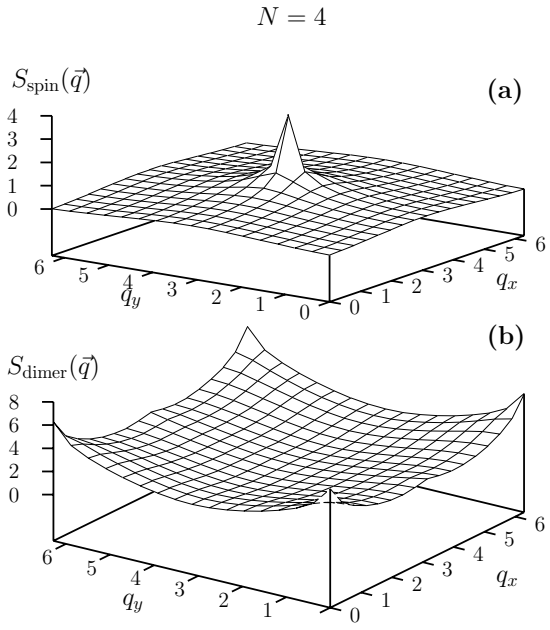

FIG. 10: Equal time dimer and spin correlation functions for the $SU(4)$ Heisenberg model.

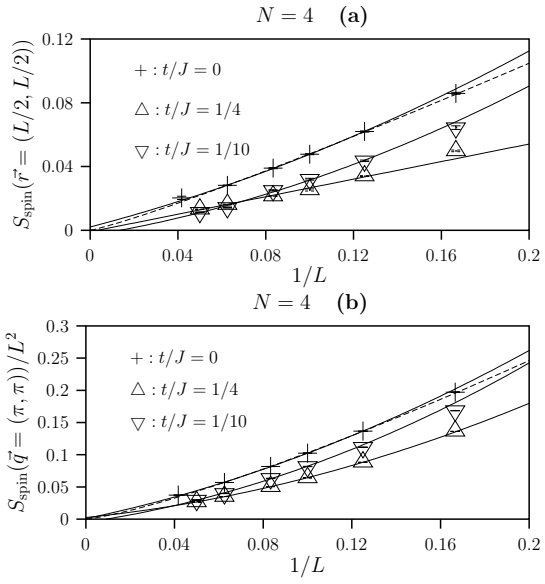

FIG. 11: Size scaling of the equal time spin-spin correlation functions. For $t/J > 0$ we set $U = 0$, and $t/J = 0$ refers to the Heisenberg model (see Sec. II C).

The data is equally consistent with a power-law decay of the spin-spin correlations. Concentrating again on the Heisenberg point the dashed lines in Fig. 11 correspond to the forms: $S_{\rm spin}(\vec{q} = (\pi, \pi))/L^2 \propto L^{-1.25}$ and $S_{\rm spin}(\vec{r} = (L/2, L/2)) \propto L^{-1.12}$. The difference between the two numerical values of the exponents gives an idea of their uncertainty.

Hence the equal time data is consistent with an insulating phase with no apparent lattice or spin symmetry breaking and no gap in the magnetic excitations. It is now intriguing to investigate the spin-dynamics of this phase. Fig. 12a plots the dynamical spin-structure factor at $t/J = 0.1$, $U/t = 0$ on a 16×16 lattice. The data, shows several features. The gap at $\vec{q} = (\pi, \pi)$ is a finite size effect (see Fig. 9b). Taking this into account, the data is consistent with a gapless mode with linear dispersion around $\vec{q} = (\pi, \pi)$. This feature is clearly not surprising since the equal time correlation functions show critical behavior at this wave vector. As we follow this mode to $\vec{q} = (0, \pi)$ the line shape becomes very broad and spectral weight seems to spill down to low energies. This is especially apparent on the intensity plot for which we have used a logarithmic scale (see Fig. 12b). Since the spectral weight of the low-lying modes around $\vec{q} = (0, \pi)$ is very small, it is desirable to confirm the above statement. To this aim we plot in Fig. 12c the imaginary time displaced correlation functions, $S_{\rm spin}(\vec{q}, \tau)$, at $\vec{q} = (0, \pi)$ and $\vec{q} = (\pi, \pi)$ both in the gapless spin-liquid phase at $t/J = 0.1$ and for comparison in the DDW phase at $t/J = 0.5$. Let us start with the DDW phase where we were able to show the presence of gapless spin modes around the (π, π), $(0, \pi)$ and $(\pi, 0)$ points in thermodynamic limit (see Fig. 6b). On the $L = 20$ sized system considered in Fig. 12c one sees that both the $\vec{q} = (0, \pi)$ and $\vec{q} = (\pi, \pi)$ correlators decay assymtotically with the same exponential form, thus signalling low energy spin excitations at both wave vectors. Of course there is a big difference in the prefactor mutiplying this exponential decay. This replects the fact that the spectral weight of the low-lying $(0, \pi)$ excitation is much smaller than

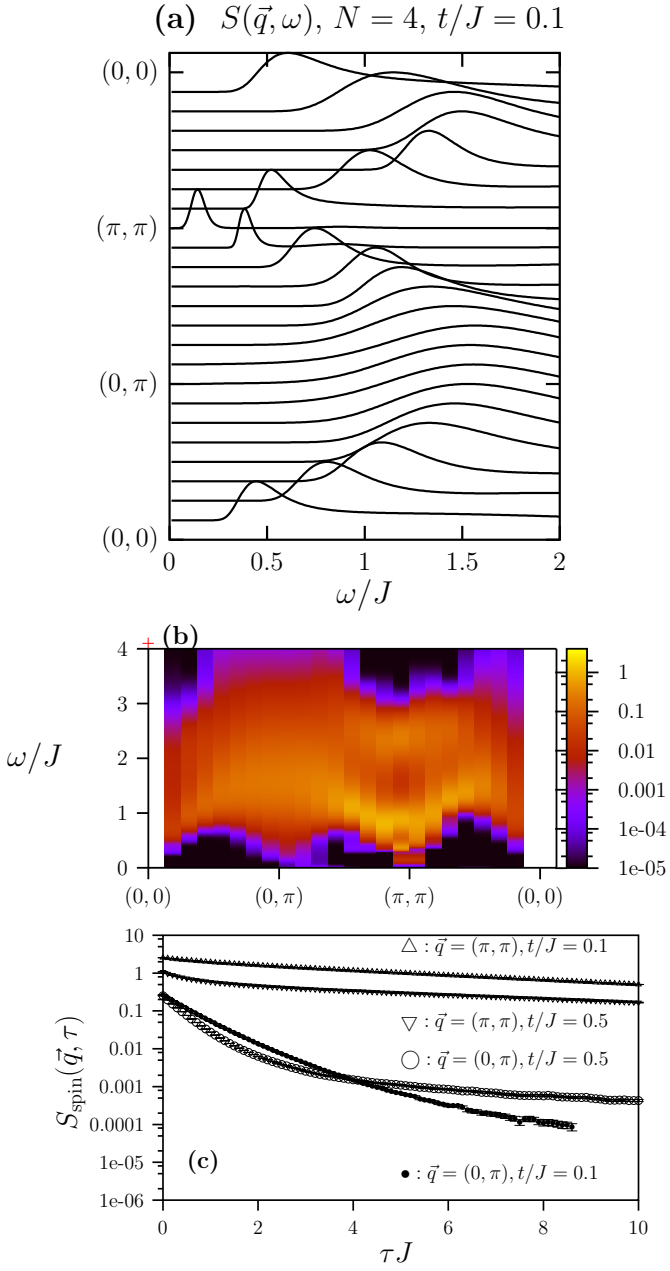

FIG. 12: (a) Dynamical spin structure factor on a 16×16 lattice. We have normalized the peak height of each spectrum to unity so as to put forward the overall shape of the dispersion relation. The reader however has to bear in mind that the weight under each spectrum is equal to the equal structure factor $S_{\rm spin}(q)$ which is peaked at $\vec{q}=(\pi,\pi)$ and vanishes at $\vec{q}=(0,0)$. (b) Intensity plot of the data of (a) on a logarithmic scale. (c) Imaginary time correlation functions. Here, one can see that without having recourse to analytical continuation, the bare imaginary time data supports the existence of low lying modes at $\vec{q}=(0,\pi)$ (See text). At $t/J=0.5$ ($t/J=0.1$) we consider a 20×20 (16×16) lattice.

that of the $\vec{q}=(\pi,\pi)$ excitation. Let us now turn our attention to the gapless spin liquid phase at $t/J=0.1$. As apparent the data shows a very similar behavior at the exception that the spectral weight at $\vec{q}=(0,\pi)$ is reduced in comparison to the DDW phase. We note that due to the extremely small scales involved in the $\vec{q}=(0,\pi)$ data at $t/J=0.1$ we are unable to obtain accurate results beyond $\tau J \simeq 8$. Hence, on the basis of this data, we believe that the spin-liquid phase indeed shows low lying spin modes not only at (π,π), but also at $(0,\pi)$ and $(\pi,0)$. Finally, we note that as we approach the Heisenberg point, the spectral weight of the low lying mode at $\vec{q}=(0,\pi)$ becomes smaller and smaller. This renders numerical detection of this feature at the Heisenberg point hard.

IV. SUMMARY AND DISCUSSION.

The half-filled $SU(N)$ Hubbard Heisenberg model shows a variety of phases, which we have analyzed in detail. The saddle point physics – a DDW phase at large values of t/J which becomes unstable to a spin dimerized state – is valid down to $N=6$. On the other hand, the $SU(2)$ model has a SDW insulating phase irrespective of the coupling constant. The most intriguing aspect of the phase diagram, is the gapless spin liquid state in the $SU(4)$ model in the vicinity of the Heisenberg point. The $SU(4)$ model has a DDW ground state at large values of t/J. As appropriate for this semi-metallic state, we find gapless single particle excitations at wave vectors $\vec{k}=(\pm\pi/2,\pm\pi/2)$. In the particle-hole channel those single particle excitations lead to gapless spin modes centered around $\vec{q}=(\pi,\pi)$, $\vec{q}=(0,\pi)$, and $\vec{q}=(\pi,0)$. Reducing the magnitude of the hopping matrix element we find a semi-metal to insulator transition. In the insulating phase the antiferromagnetic, $\vec{Q}=(\pi,\pi)$, spin correlations are critical and for the $SU(4)$ Heisenberg model the data is consistent with the form $S_{\rm spin}(\vec{r}) \sim e^{i\vec{Q}\cdot\vec{r}}|\vec{r}|^{-1.12}$. This state shows no lattice broken symmetries and hence is a candidate for a gapless spin liquid state. In the particle-hole channel, the dynamical spin structure factor points to gapless excitations at $\vec{q}=(\pi,\pi)$ but also to low-lying modes with small spectral weight centered around $\vec{q}=(0,\pi)$ and $\vec{q}=(\pi,0)$.

It is tempting to argue that the gapless spin liquid phase is well described by a DDW mean-field state supplemented with a Gutzwiller projection. Requiring invariance under time reversal symmetry pins the flux in each elementary square to π. Clearly, the Gutzwiller projection triggers the semi-metal to insulator transition but one could argue that in the particle-hole channel excitations remain gapless such that low lying spin excitations are present at wave vectors $\vec{q}=(\pi,\pi)$, $\vec{q}=(0,\pi)$, and $q=(\pi,0)$. In the $SU(2)$ case, this variational wave function has been investigated in details. It turns out that due to a local $SU(2)$ symmetry [14] it is equivalent to a BCS $d-$wave Gutzwiller projected wave function

[15]. At the particle-hole symmetric point the equal time spin-spin correlations of this wave function have been computed [16] to obtain a power-law decay of the antiferromagnetic correlations: $S(\vec{r}) \sim e^{i\vec{Q}\cdot\vec{r}}|\vec{r}|^{-1.5}$. Furthermore, the spin structure factor as computed form the variational wave function shows no cusp feature at $\vec{q} = (0, \pi)$ and $\vec{q} = (\pi, 0)$ [22]. This result compares favorably with behavior of the spin-spin correlations in the $SU(4)$ Heisenberg model discussed in the present work.

Alternatively we can ask the question of whether or not our results for the $SU(4)$ Heisenberg model are understandable from the perspective of the large-N saddle point. In the large-N limit and at the Heisenberg point one can stabilize the π-flux phase by adding biquadratic terms to the Hamiltonian [10]. Furthermore, Hemerle et al. [17] have argued in favor of the stability of the π-flux phase to gauge fluctuations arising from the constraint of no double occupancy. At the mean-field level, the π-flux phase shows antiferromagnetic spin-spin correlations which decay as $S(\vec{r}) \sim e^{i\vec{Q}\cdot\vec{r}}|\vec{r}|^{-4}$. Including gauge fluctuations in a $1/N$ approximation reduces the mean field exponent [18]. On the other hand, the $(0, \pi)$ spin-spin correlations remain unaffected by gauge fluctuations [18]. Those results compare favorably with our calculations at $N = 4$.

To investigate the nature of the spinless liquid state we find in the $SU(4)$ Heisenberg model, it is desirable to investigate it's behavior under perturbations. Following the variational work of [16, 19], the particle-hole symmetric point is unstable towards a Z_2 spin liquid as realized for example in quantum dimer models [20]. This instability is triggered by the inclusion of a next nearest neighbor hopping matrix element in the BCS Slater determinant. In the spin model this translates in the inclusion of a frustrating exchange coupling. Unfortunately, this is not accessible to the quantum Monte Carlo approach since frustration leads to a minus sign problem. Another perturbation, which is accessible to the Monte Carlo approach, is the inclusion of a uniform magnetic field. Based on the mean-field description of the π-flux phase, we can speculate that the point-like Fermi *surface* at zero field evolves to rings around centered around the zero field nodes. Since we are at a particle-hole symmetric point and that this symmetry is not broken under the inclusion of a magnetic field, the finite field Fermi surface is unstable towards magnetic ordering. Very much as in discussed in Ref. [21] this produces a field induced transition to an magnetically ordered state.

Acknowledgments. The calculations presented here were carried out on the IBM p690 cluster of the NIC in Jülich. I would like to thank this institution for generous allocation of CPU time. Part of this work has been carried out at the KITP, in the framework of a program on Exotic order and Criticality in Quantum Matter. I have greatly profited from discussions with M. Hermele, M. Imada. B. Marston, G. Misguich, A. Paramekanti, S. Sachdev and J. Zaanen. This research was supported in part by the National Science Foundation under Grant No. PHY99-07949.

[1] K. I. Kugel' and D. I. Khomskii, Sov. Phys. Usp. **25**, 232 (1982).
[2] Y. Q. Li, M. Ma, D. N. Shi, and F. C. Zhang, Phys. Rev. Lett. **81**, 3527 (1988).
[3] C. Honerkamp and W. Hofstetter, Phys. Rev. Lett. (2004).
[4] F. F. Assaad, V. Rousseau, F. Hébert, M. Feldbacher, and G. Batrouni, Europhys. Lett. **63**, 569 (2003).
[5] C. Wu, J. P. Hu, and S. C. Zhang, Phys. Rev. Lett. **91**, 186402 (2003).
[6] N. Read and S. Sachdev, Nucl. Phys. B **316**, 609 (1989).
[7] G. Santoro, S. Sorella, L. Guidoni, A. Parola, and E. Tosatti, Phys. Rev. Lett. **83**, 3065 (1999).
[8] K. Harada, N. Kawashima, and M. Troyer, Phys. Rev. Lett. **90**, 117203 (2003).
[9] I. Affleck and J. B. Marston, Phys. Rev. B **37**, 3774 (1988).
[10] J. B. Marston and I. Affleck, Phys. Rev. B **39**, 11538 (1989).
[11] T. Dombre and G. Kotliar, Phys. Rev. B **38**, 855 (1989).
[12] S. Capponi and F. F. Assaad, Phs. Rev. B **63**, 155114 (2001).
[13] D. Arovas and A. Auerbach, Phs. Rev. B **38**, 316 (1998).
[14] I. Affleck, Z. Zou, T. Hsu, and P. Anderson, Phys. Rev. B **38**, 745 (1988).
[15] C. Gross, Phys. Rev. B **38**, 931 (1988).
[16] A. Paramekanti, M. Randeria, and N. Trivedi, http://xxx.lanl.gov/cond-mat/0405353 .
[17] M. Hermele, T. Senthil, M. P. A. Fisher, P. A. Lee, N. Nagaosa, and X. G. Wen, http://xxx.lanl.gov/cond-mat/0404751 .
[18] W. Rantner and X. Wen, Phys. Rev. B **66**, 144501 (2002).
[19] D. Ivanov and T. Senthil, Phys. Rev. B **66**, 115111 (2002).
[20] G. Misguich, D. Serban, and V. Pasquier, Phys. Rev. Lett. **89**, 137202 (2002).
[21] I. Milat, F. Assaad, and M. Sigrist, http://xxx.lanl.gov/cond-mat/0312450 .
[22] A. Paramekanti, private communication